Spontaneous pattern formation and genetic invasion in locally mating and competing populations

Hiroki Sayama,[1,2] Marcus A. M. de Aguiar,[1,3,4] Yaneer Bar-Yam,[1,5] and Michel Baranger[1,4]
[1]*New England Complex Systems Institute, Cambridge, Massachusetts 02138*
[2]*Department of Human Communication, University of Electro-Communications, Chofu, Tokyo 182-8585, Japan*
[3]*Instituto de Física "Gleb Wataghin," Universidade Estadual de Campinas, 13081-970, Campinas, São Paulo, Brazil*
[4]*Center for Theoretical Physics and Laboratory of Nuclear Science, Massachusetts Institute of Technology, Cambridge, Massachusetts 02139*
[5]*Department of Molecular and Cellular Biology, Harvard University, Cambridge, Massachusetts 02138*
(Received 19 December 2001; published 17 May 2002)

We present a theoretical model of evolution of spatially distributed populations in which organisms mate with and compete against each other only locally. We show using both analysis and numerical simulation that the typical dynamics of population density variation is a spontaneous formation of isolated groups due to competition for resources. The resulting spatial separation between groups strongly affects the process of genetic invasion by local reproductive mixing, and spatially inhomogeneous genetic distributions are possible in the final states. We then consider a specific version of this model in the presence of disruptive selection, favoring two fittest types against their genetic intermediates. This case can be simplified to a system that involves just two nonconserved order parameters: population density and type difference. Since the coexistence of two fittest types is unstable in this case, symmetry breaking and coarsening occur in type difference, implying eventual dominance by one type over another for finite populations. However, such coarsening patterns may be pinned by the spontaneously generated spatial separation between isolated groups. The long-term evolution of genetic composition is found to be sensitive to the ratio of the mating and competition ranges, and other parameters. Our model may provide a theoretical basis for consideration of various properties of spatially extended evolutionary processes, including spontaneous formation of subpopulations and lateral invasion of different types.

DOI: 10.1103/PhysRevE.65.051919 PACS number(s): 87.23.Cc, 87.23.Kg, 89.75.Kd

I. INTRODUCTION

Species in the wild display spatial variations. Such variability is commonly attributed to variations in selective forces, i.e., differences in the environment. However, spatially distributed systems can develop inhomogeneity through symmetry breaking and spontaneous pattern formation independently of environmental inhomogeneity. Typically, the existence of local but spatially overlapping mating neighborhoods (demes) in a two-dimensional space may result in a dynamic pattern of polymorphism, and the evolution of the patterns is then controlled by the kinetics of boundaries between different types [1]. The significance of such spatial patterns in ecological processes was realized fairly recently and they were introduced in various studies [2–6]. On the other hand, analogous studies of dynamic spatial patterns in evolutionary genetics are just beginning [1,7]. Most of the results obtained in both kinds of studies can be approximately described with a single nonconserved order parameter (e.g., type of organisms), resulting in several well-known system behaviors such as symmetry breaking and coarsening or nucleation and growth, depending on fitness assignments and initial conditions.

In this paper, we extend the understanding of the dynamics of pattern formation in spatially distributed evolutionary processes by considering a more general case that involves population density variation as well as genetic or type variation. The underlying dynamics of this model correspond to the formation of isolated groups through population density variation and, in the presence of disruptive selection, symmetry breaking and coarsening through type difference. For each parameter setting, we study the regimes in which patterns form and the characteristic wavelengths of the patterns, using linear stability analysis. Numerical simulations confirm these analytical results, and furthermore demonstrate how the evolution of genetic variation interacts with population density variation. The ratio of the two key length scales in the problem, the mating range and the competition range, plays a crucial role in the long-term evolution of the patterns.

These results have several important implications for spatially extended evolutionary processes. In particular, they are relevant to the processes of spontaneous formation of subpopulations and lateral invasion of different types, which has been a subject of particular interest in population genetics and evolutionary biology [8,9].

In Sec. II we introduce the model. Section III is the analysis of its basic dynamics with no fitness variation between different genotypes. In Sec. IV, we consider a special case of the model, where genetic intermediates are assumed not viable. Finally, in Sec. V, we discuss several implications of our results.

II. GENERAL MODEL

We start with a population with local genetic mixing by sexual reproduction and local competition for finite resources necessary for reproduction. We restrict ourselves to a simple genetic model where a genome is made of two genes, each of which is one of two allelic types ($+$ and $-$) and is inherited from one of the two parents participating in sexual reproduc-

tion. Thus there are four possible genotypes $[++]$, $[+-]$, $[-+]$, and $[--]$. Biologically speaking, this can be viewed as two-locus haploid genetics where gene recombination is enforced in every mating, or as one-locus diploid genetics if $[+-]$ and $[-+]$ are identified with each other. For simplicity, we assume that organisms are monoecious, i.e., any pair of individuals can mate to produce offspring. The specifics of the model are as follows.

(1) Organisms are distributed over a two-dimensional discrete grid.

(2) The local populations on each site in the grid are characterized by non-negative real numbers with no predefined upper bound.

(3) At each discrete time step (breeding season), offspring are born and part of the previous population dies.

(4) Genetic mixing by sexual reproduction takes place within local mating neighborhoods (demes) that range over several sites.

(5) The total number of offspring born per site per season is bounded by the introduction of an intrinsic carrying capacity (limitation of resources for reproduction).

(6) Competition for limited resources takes place within local competition neighborhoods ranging over several sites, whose size may be different from that of the mating neighborhoods.

The general form of the iterative equation of local populations on each site is

$$n'_{ab}(\boldsymbol{x}) = \sigma_{ab} n_{ab}(\boldsymbol{x}) + \lambda_{ab} \langle n(\boldsymbol{x}) \rangle_M \times \frac{\langle n_{a*}(\boldsymbol{x}) \rangle_M}{\langle n(\boldsymbol{x}) \rangle_M} \frac{\langle n_{*b}(\boldsymbol{x}) \rangle_M}{\langle n(\boldsymbol{x}) \rangle_M} \left[1 - \frac{\langle n(\boldsymbol{x}) \rangle_C}{\kappa} \right], \quad (1)$$

which simplifies to

$$n'_{ab}(\boldsymbol{x}) = \sigma_{ab} n_{ab}(\boldsymbol{x}) + \frac{\lambda_{ab} \langle n_{a*}(\boldsymbol{x}) \rangle_M \langle n_{*b}(\boldsymbol{x}) \rangle_M}{\langle n(\boldsymbol{x}) \rangle_M} \times \left[1 - \frac{\langle n(\boldsymbol{x}) \rangle_C}{\kappa} \right]. \quad (2)$$

The notation is as follows. $n_{ab}(\boldsymbol{x})$ (a,b are either $+$ or $-$) is the local population of genotype $[ab]$ at site $\boldsymbol{x}$, with the constraint $n_{ab} \geqslant 0$. $n \equiv n_{++} + n_{+-} + n_{-+} + n_{--}$, $n_{a*} \equiv n_{a+} + n_{a-}$, $n_{*b} \equiv n_{+b} + n_{-b}$. The primes on the left hand sides of Eqs. (1) and (2) denote the value after a unit of time. σ_{ab} is the survival rate of parents of genotype $[ab]$, and λ_{ab} is their reproductive rate (the number of offspring born per parent per season). These rates are bounded so that $0 < \sigma_{ab} < 1$ and $\lambda_{ab} > 0$. M is the mating neighborhood, and C is the competition neighborhood. We assume that M and C are a set of relative coordinates of sites in a pseudocircular region centered at the site, whose radius is R_M or R_C and whose edges are jagged (not a perfect circle) along a discrete square spatial lattice. κ is the carrying capacity per site. Each pair of angular brackets on the right hand side represents the local average of the given function in the neighborhood around $\boldsymbol{x}$, i.e., $\langle f(\boldsymbol{x}) \rangle_N \equiv [\Sigma_{\boldsymbol{r} \in N} f(\boldsymbol{x}+\boldsymbol{r})]/|N|$, where $|N|$ is the number of sites included in the neighborhood N. The terms inside the square brackets on the right hand side of Eqs. (1) and (2) describe a logistic growth restriction on the population at local sites due to the already existing population in their vicinity. They apply only to reproduction, modeling the fact that adult individuals usually have a large advantage when competing with newborns.

Explained intuitively, this equation implies that if the limitation on population by competition is ignored, $(1-\sigma)$ of the population at a particular site will die and λ of the average population within its local mating neighborhood will be born in each breeding season. The genetic composition of the newborns is determined in Eq. (1) by including the product of two allelic probabilities observed within the mating neighborhood.

III. FLAT FITNESS CASE

A. Model

We begin by analyzing the underlying dynamics of Eq. (2), assuming $\sigma_{ab} = \sigma$ and $\lambda_{ab} = \lambda$ for all a,b. This is the reference case where there is no difference in fitness (i.e., reproduction and survival rates) among all the four genotypes, which we call the *flat fitness case*. For simplicity, we measure the populations in units of the carrying capacity κ.

Using these assumptions, summing up both sides of Eq. (2) for all genotypes gives

$$n'(\boldsymbol{x}) = \sigma n(\boldsymbol{x}) + \lambda \langle n(\boldsymbol{x}) \rangle_M [1 - \langle n(\boldsymbol{x}) \rangle_C] \quad (3)$$

with the constraint $n \geqslant 0$. This is a simplified equation for the population density only, independent of genetic composition. In Secs. III B–III D we consider the basic properties of the evolution of population density variation, using Eq. (3).

B. Homogeneous solutions

We first study the spatially homogeneous solutions of Eq. (3). This can be viewed either as a type of mean field approximation, or as a panmictic limit where the mating and competition neighborhoods extend over all available space. In this case the averages over M and C are not necessary and Eq. (3) is simplified to

$$n' = \sigma n + \lambda n (1-n). \quad (4)$$

This gives two stationary solutions, $n=0$ and $n=(\sigma+\lambda-1)/\lambda$. The first corresponds to extinction. The second is a nontrivial solution, which we call n_0. Defining $\alpha \equiv \sigma + \lambda$ and $q \equiv \lambda n/\alpha$, Eq. (4) becomes

$$q' = \alpha q (1-q), \quad (5)$$

which is the well-known logistic map [10,11]. We note that α is the net growth rate of the population that includes both survival of the parents and birth of the offspring. The stationary solutions are $q=0$ and $q=(\alpha-1)/\alpha \equiv q_0$, corresponding to the above two solutions, respectively. The first (trivial) solution is stable if $\alpha < 1$. The second solution $q=q_0$ is

stable if $1<\alpha<3$. At $\alpha=3$, however, this solution undergoes a period doubling bifurcation, followed by the well-known cascade of period doublings as α increases, leading to chaos. Thus we obtain the following three regimes for the basic properties of evolutionary outcome of population density variation in terms of the net growth rate $\sigma+\lambda$. (I) $\sigma+\lambda<1$; only extinction is possible, as an attractor for any initial condition. (II) $1<\sigma+\lambda<3$; extinction is unstable and the nontrivial solution n_0 is stable. (III) $\sigma+\lambda>3$; the solution n_0 undergoes period-doubling bifurcations beginning at $\sigma+\lambda=3$, leading to chaos.

C. Stability analysis of the spatially extended version

When the population is spatially extended with local mating/competition ranges, the homogeneous solutions obtained above may not apply because local symmetry breaking can give rise to spontaneous pattern formation and significant spatial inhomogeneities. In this section we study the pattern formation process in population density using linear stability analysis with space-dependent perturbations, and its dependence on σ, λ, R_M, and R_C.

We consider a two-dimensional oscillatory perturbation added to n_0, with wave vector v for the x direction and w for the y direction. We write the time evolution of perturbation in a two-dimensional population as

$$n^t(x,y)=n_0+\xi\mu^t s(x,y) \tag{6}$$

with

$$s(x,y)=\sin(vx+\phi)\sin(wy+\psi), \tag{7}$$

where ξ is a small amplitude. The homogenous solutions are unstable and patterns form when μ is greater than 1. Substituting Eq. (6) into Eq. (3) and keeping only linear (first-order) terms of ξ, we obtain

$$n^{t+1}(x,y)=n_0+\xi\mu^t[\sigma s(x,y)+(1-\sigma)\langle s(x,y)\rangle_M - (\sigma+\lambda-1)\langle s(x,y)\rangle_C]. \tag{8}$$

To calculate μ we approximate the averages over the discrete neighborhoods M and C using integrals over continuous circular neighborhoods, assuming that R_M and R_C are not too small. Using polar coordinates, we analytically obtain

$$\langle s(x,y)\rangle_N \approx \frac{1}{\pi R_N^2}\int_0^{R_N}\int_0^{2\pi}\sin(vx+\phi+vr\cos\theta)\times\sin(wy+\psi+wr\sin\theta)\,d\theta\,r\,dr = \frac{2s(x,y)J_1(fR_N)}{fR_N}, \tag{9}$$

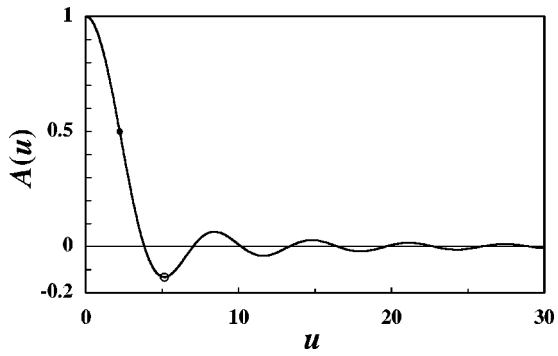

FIG. 1. Numerical plot of $A(u)$ in Eq. (11) for $u>0$. The global minimum $(u_0,z_0)\approx(5.135\,62,-0.132\,279)$ is marked with an open circle. The point $(u_c,1/2)\approx(2.215\,09,0.5)$ that satisfies $A(u)=1/2$ is marked with a closed circle.

where $f\equiv\sqrt{v^2+w^2}$ is the magnitude of the two-dimensional wave vector ($v=f\cos\rho, w=f\sin\rho$), and J_n is the Bessel function of the first kind of order n. Applying this approximation to Eq. (8), we obtain

$$\mu=\sigma+(1-\sigma)A(fR_M)-(\sigma+\lambda-1)A(fR_C) \tag{10}$$

with

$$A(u)\equiv\frac{2J_1(u)}{u}. \tag{11}$$

The actual shape of $A(u)$ is plotted in Fig. 1 for $u>0$. This function has a conspicuous minimum at $u\approx5.135\,62$ where $A(u)\approx-0.132\,279$, which we call u_0 and z_0 in what follows.

The condition for the homogeneous solution to be unstable is that there are some values of f that satisfy $|\mu|>1$. Here we focus on the more relevant case $\mu>1$. Note that μ smaller than -1 is also possible for sufficiently small σ and large λ in our model. However, it gives rise to a pattern that inverts itself at each unit of time, which is not as relevant to modeling ecological populations. For $\mu>1$, the condition for instability is the existence of such values of u that satisfy

$$\delta A(u/\gamma)<A(u)-1, \tag{12}$$

where $u\equiv fR_M$, $\gamma\equiv R_M/R_C$, and $\delta\equiv(\sigma+\lambda-1)/(1-\sigma)$. Since it is hard to obtain the analytical solution of this inequality, we use the following approximation: When parameters γ and δ gradually move from stable regimes, the value of u that first satisfies this inequality should be obtained near the minimum of its left hand side. Specifically, the minimum is at $u=\gamma u_0$ where $\delta A(u/\gamma)=\delta z_0$. Using these assumptions, the condition for the inequality to be satisfied is given by

$$\delta z_0<A(\gamma u_0)-1. \tag{13}$$

Figure 2(a) shows the regimes where this condition is, or is not, satisfied in the (γ,δ) plane. We see that, as the mating range becomes smaller than the competition range, the ho-

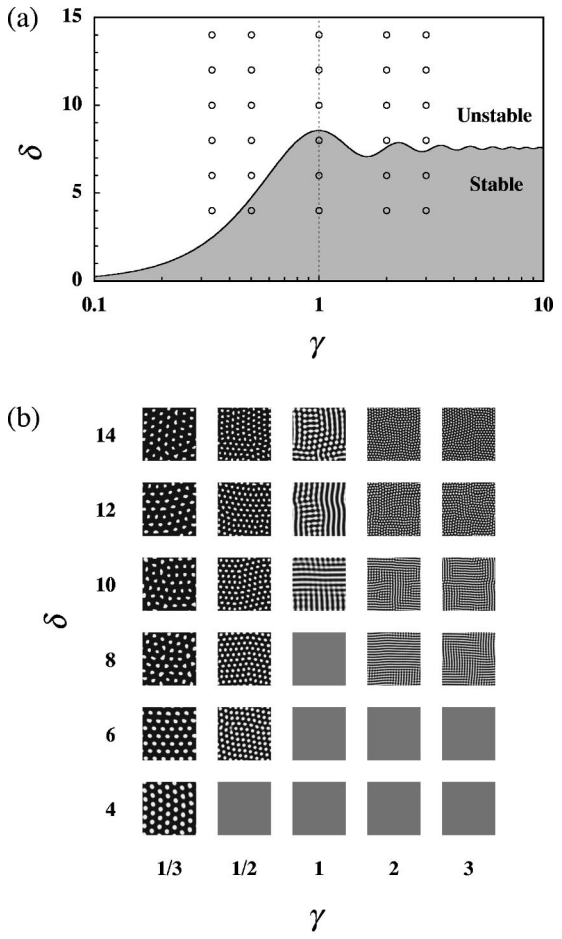

FIG. 2. (a) Phase diagram in the (γ,δ) plane showing the stability of the homogeneous solution obtained from the inequality (13). In the shaded region below the curve, $\delta z_0 > A(\gamma u_0) - 1$, which implies that the homogeneous solution is stable, while above the curve it is not. Open circles are the sample points chosen to generate the simulation results shown below. (b) Numerical simulation results of pattern formation in population density in the flat fitness case. Each picture represents a snapshot of the evolution of spatial patterns for each sample case (shown above), taken after 500 updates. The space consists of 128×128 sites with periodic boundary conditions. Each picture shows a configuration of the entire space. The brightness at each pixel represents the local population density. σ is set to 0.9 for all cases. λ is varied to obtain different values of δ. The values of (R_M, R_C) used here are (5,15) for $\gamma = 1/3$, (5,10) for $\gamma = 1/2$, (10,10) for $\gamma = 1$, (10,5) for $\gamma = 2$, and (15,5) for $\gamma = 3$. Initial conditions are randomly generated populations with $n = 0.1\kappa$ (with $\pm 0.02\kappa$ fluctuations) for each site.

mogeneous solution can be destabilized, while if the mating range is greater than the competition range, the stability of the homogeneous solution is determined almost solely by δ. Numerical results of spatially explicit simulations are shown in the same figure for several different γ and δ [Fig. 2(b)], implying that our analysis closely corresponds to the actual model behavior. The existence of an instability is seen as the formation of isolated groups (spots or stripes), similar to the well-known Turing patterns caused by local activation and long-range inhibition in reaction-diffusion systems [12–14]. The characteristic length scale of these patterns does not depend on system size for systems larger than this length scale, because the system is only unstable to perturbations over a finite range of wavelengths [15].

From numerical simulations we also find that even populations that would be in the bifurcation or chaotic regimes in the previous analysis of the homogeneous case actually result in static patterns in the spatially extended case. Such deviation from the mean-field result in spatially extended settings is also reported for other oscillating reaction-diffusion models [16,17], where homogeneous oscillations are destroyed by stochastic disturbances added to local phases and thus no coherent behavior is seen at large scales. Our model is distinct from those models because its underlying dynamics is not oscillatory but of logistic growth, and, when extended spatially, the generated patterns become static even at small scales due to significant inhomogeneities in population density created by local symmetry breaking. In addition, for $\gamma \geqslant 1$, the resultant patterns vary from stripes to spots as δ deviates from its critical values near the instability curve.

Finally, we calculate the characteristic wavelength of the patterns, which we call L. We note that the characteristic scale is determined by the wave vectors of the perturbations that maximize μ shown in Eq. (10). With the notation $u \equiv f R_M$, Eq. (10) becomes

$$\mu = \sigma + (1-\sigma)[A(u) - \delta A(u/\gamma)]. \tag{14}$$

Assuming that δ is much greater than 1 for most parameter settings being studied (see Fig. 2), we approximate the value of u that maximizes μ by the value that minimizes $\delta A(u/\gamma)$. We obtain $u \approx \gamma u_0$, and hence $f \approx \gamma u_0 / R_M \equiv f_0$, as an approximate value of f that determines the wavelength of the patterns.

Since there are many different perturbations that take the same particular value for f, we need to compute which wave vector is dominant in the patterns that superimpose all such perturbations. To do this we first consider what wave vectors exist in the perturbation $s(x,y)$ along the direction of observation $(x_\omega, y_\omega) = (\tau\cos\omega, \tau\sin\omega)$. Using the same notation as before, $v = f\cos\rho$ and $w = f\sin\rho$, we obtain

$$\begin{aligned} s(x_\omega, y_\omega) &= \sin(v x_\omega + \phi)\sin(w y_\omega + \psi) \\ &= \sin(\tau f \cos\rho\cos\omega + \phi) \\ &\quad \times \sin(\tau f \sin\rho\sin\omega + \psi) \\ &= -\frac{1}{2}\cos[\tau f\cos(\rho-\omega) + \phi + \psi] \\ &\quad + \frac{1}{2}\cos[\tau f\cos(\rho+\omega) + \phi - \psi], \end{aligned} \tag{15}$$

which implies that the perturbation at the angle ω contains two distinct wave vectors $f\cos(\rho-\omega)$ and $f\cos(\rho+\omega)$ with the same amplitude. Integrating the power spectrum over all angles eliminates both ρ and ω from the expression and gives

$$S(k)=\begin{cases}\dfrac{2}{\sqrt{f^2-k^2}} & (-f<k<f)\\ 0 & (\text{otherwise}),\end{cases} \tag{16}$$

which diverges to $+\infty$ as k approaches $\pm f$, implying that the dominant wave vector of the pattern is f. Therefore, the characteristic wavelength of the pattern is calculated using f_0 to be

$$L\equiv\frac{2\pi}{f_0}=\frac{2\pi R_M}{\gamma u_0}=\frac{2\pi R_C}{u_0}\approx 1.223\,45R_C, \tag{17}$$

which coincides with the numerical results shown in Fig. 2(b). Note that L depends only on the competition range and not on the mating range. This is due to the assumption $\delta \gg 1$ which we used to simplify Eq. (14), and thus it may not apply to other cases.

D. Sensitivity to the neighborhood shape

An interesting characteristic of the present model is its sensitivity to the shape of neighborhoods. In the calculations presented above, we have adopted ''circular'' neighborhoods, where the average of a function $f(\boldsymbol{x})$ is defined, using weight function W_N, by

$$\langle f(\boldsymbol{x})\rangle_N=\frac{\sum_{\boldsymbol{r}} f(\boldsymbol{x}+\boldsymbol{r})W_N(\boldsymbol{r})}{\sum_{\boldsymbol{r}} W_N(\boldsymbol{r})}, \tag{18}$$

where $W_N(\boldsymbol{r})=1$ if $|\boldsymbol{r}|<R_N$ and is otherwise 0. We have tested other possibilities such as ''square'' neighborhoods or ''Gaussian'' neighborhoods. The square neighborhoods, obtained by redefining $W_N(\boldsymbol{r})=1$ if $\max(|r_x|,|r_y|)<R_N$ and is otherwise 0, give results that are very similar to those obtained from circular neighborhoods. However, this is not the case for the Gaussian neighborhoods with $W_N(\boldsymbol{r})=e^{-(|\boldsymbol{r}|/R_N)^2}$. In this case, the homogeneous solution is stable against perturbation of any wavelength in population density. Mathematically, this can be understood by noting that the integral of sine functions with Gaussian weights, which is a Fourier transform, is again a Gaussian. This cannot be negative, in contrast to the function $A(u)$ shown in Fig. 1. Therefore the average of the perturbation at a given point always has the same sign as the perturbation itself at that point. Even if the perturbation is very small, the average cannot reverse its sign and destructive interference cannot happen in population density, therefore spatial separation does not take place.

From a biological point of view, this result means that isolated groups may or may not form depending on the organismal territorial behavior. In particular, when the range of foraging or mating is well defined, groups may form. If they are too smooth, e.g., if organisms diffuse in a random fashion (which results in Gaussian neighborhoods), groups will not form. This prediction could, in principle, be verified experimentally.

We also note that the stability characteristics of genetic composition, which will be discussed in the following sections, are robust to the neighborhood shape variations.

E. Genetic invasion

The discussion thus far does not include the dynamics of genetic composition. In this section we investigate the genetic composition variations within the population and how they are affected by the population structure created by competition, and its dependence on γ. We find simple genetic diffusion when γ is greater than a certain critical value; otherwise genetic decoupling is found between isolated groups.

We first calculate the probability of each genotype $p_{ab}\equiv n_{ab}/n$ for sites where organisms exist ($n>0$), by dividing Eq. (2) with Eq. (3), resulting in

$$p'_{ab}(\boldsymbol{x})=p_{ab}(\boldsymbol{x})+\frac{Q(\boldsymbol{x})}{\sigma+Q(\boldsymbol{x})}\times[P^M_{a*}(\boldsymbol{x})P^M_{*b}(\boldsymbol{x})-p_{ab}(\boldsymbol{x})] \tag{19}$$

with

$$Q(\boldsymbol{x})\equiv\frac{\lambda\langle n(\boldsymbol{x})\rangle_M}{n(\boldsymbol{x})}[1-\langle n(\boldsymbol{x})\rangle_C], \tag{20}$$

$$P^M_{a*}(\boldsymbol{x})\equiv\frac{\langle n_{a*}(\boldsymbol{x})\rangle_M}{\langle n(\boldsymbol{x})\rangle_M}, \tag{21}$$

$$P^M_{*b}(\boldsymbol{x})\equiv\frac{\langle n_{*b}(\boldsymbol{x})\rangle_M}{\langle n(\boldsymbol{x})\rangle_M}. \tag{22}$$

$P^M_{a*}(\boldsymbol{x})$ is the probability of allele a observed at the first locus within M around $\boldsymbol{x}$, and similarly $P^M_{*b}(\boldsymbol{x})$ of allele b at the second locus. For populations that do not exceed the carrying capacity, $Q(\boldsymbol{x})/[\sigma+Q(\boldsymbol{x})]$ is always positive and thus p_{ab} always approaches $P^M_{a*}P^M_{*b}$, which is a ''balanced'' probability of genotype $[ab]$ with linkage equilibrium that assumes no correlation between the probabilities of a and b within the neighborhood.

If the mean-field approximation is applied to Eq. (19), assuming that the local population within M is almost uniform, we obtain

$$p'_{ab}=p_{ab}+\frac{Q}{\sigma+Q}[p_{a*}p_{*b}-p_{ab}]=(1-\epsilon)p_{ab}+\epsilon p_{a*}p_{*b}, \tag{23}$$

where $p_{a*}=p_{a+}+p_{a-}$, $p_{*b}=p_{+b}+p_{-b}$, and $\epsilon\equiv Q/[\sigma+Q]$. Using this equation, we find that

$$
\begin{aligned}
p'_{a*} &= p'_{a+} + p'_{a-} \\
&= (1-\epsilon)p_{a+} + \epsilon p_{a*}p_{*+} + (1-\epsilon)p_{a-} + \epsilon p_{a*}p_{*-} \\
&= (1-\epsilon)p_{a*} + \epsilon p_{a*}p_{**} \\
&= p_{a*}, \qquad (24)
\end{aligned}
$$

and similarly $p'_{*b} = p_{*b}$. These results imply that both allelic frequencies p_{a*} and p_{*b} are conserved over time. This result is known as the Hardy-Weinberg law in population genetics. It implies that any change in the average genetic composition within the mating neighborhood will be preserved, affecting the future genetic composition at the center of the neighborhood. Therefore, when there is variation in genetic composition between nearby local populations with partial genetic mixing, they mutually influence each other's genetic composition and converge toward the same intermediate composition. Moreover, if all the organisms are reproductively connected in the long term (i.e., if genetic mixing is possible between descendants of any pair of organisms), the whole population tends toward genetic homogenization in equilibrium.

As we saw in the previous discussion, there are also regimes where local competition spontaneously generates isolated population groups. If the width of the spatial separation between these groups is large enough so that organisms in one group cannot find others in different groups within their mating neighborhood M, then $P^M_{a*}(\boldsymbol{x})P^M_{*b}(\boldsymbol{x})$ in Eq. (19) becomes a balanced probability *within* that group, i.e., groups are genetically decoupled from each other. In such a regime an inhomogeneous genetic distribution may be the final steady state of the population. We compute the critical ratio of the mating and competition ranges γ_c (below which groups become genetically decoupled after pattern formation) by assuming that the spatial separation is about half as wide as the characteristic wavelength L. This approximation yields

$$\gamma_c \approx \frac{L}{2R_C} \approx 0.612. \qquad (25)$$

Figure 3 shows several results of numerical simulations with genetically inhomogeneous initial populations, which appear to be consistent with the approximate value of γ_c obtained above.

To summarize, in the flat fitness case, the underlying dynamics of spatial variation in genetic composition is a simple genetic diffusion by local reproductive mixing. Without spatial separation, it leads to a complete homogenization of genetic composition over the entire population. However, with spatial separation due to competition for resources, genetic invasion is affected by the length scale of the patterns, depending on whether the ratio of the mating and competition ranges is larger than its critical value γ_c. For $\gamma < \gamma_c$, spatially inhomogeneous genetic distributions are possible in the final states.

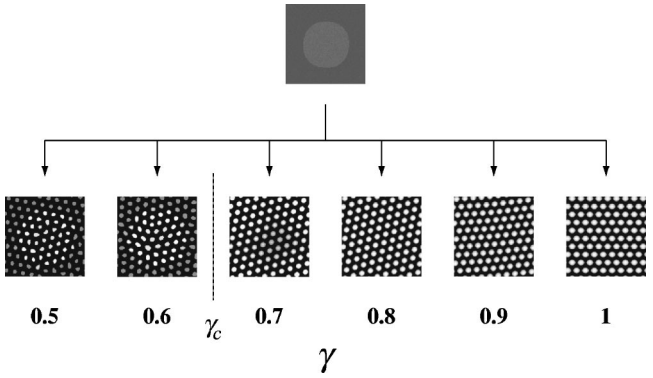

FIG. 3. Results of numerical simulations showing the population density for several different values of γ in the flat fitness case, starting from a genetically inhomogeneous initial condition. The space consists of 128×128 sites with periodic boundary conditions. Each picture shows a configuration of the entire space. Dark gray represents the existence of $[++]$ organisms, light gray represents the existence of $[--]$, and black represents empty (or nearly empty) regions. $\sigma = 0.9$ and $\lambda = 1.5$ so that $\delta = 14$. R_C is fixed to 10, while R_M is varied to obtain different values of γ. The top picture is the initial condition, where a circular region of $[--]$ organisms is placed in a background population of $[++]$ organisms. Population density is initialized so that $n = 0.1\kappa$ (with $\pm 0.02\kappa$ fluctuations) for each site. Each picture at the bottom represents a snapshot of the evolution of spatial patterns for each value of γ, taken after 3000 updates. Genetic homogenization can be seen for $\gamma > \gamma_c \approx 0.612$, while a nonhomonegenous genetic distribution remains for $\gamma < \gamma_c$.

IV. DISRUPTIVE SELECTION CASE

A. Model

The implications of pattern formation for genetic invasion discussed in the previous section may not apply if there are differences in fitness among distinct genotypes. In Sec. IV we consider the dynamics of genetic invasion in the presence of disruptive selection (selection against genetic intermediates) by assuming that genotypes $[+-]$ and $[-+]$ are not viable, i.e., $\sigma_{+-} = \sigma_{-+} = \lambda_{+-} = \lambda_{-+} = 0$. Disruptive selection arises in various conditions in nature, such as competition for diverse resources or mutual dependence of multiple phenotypes [18], and is viewed as one of the most general and important causes of inhomogeneity generation, including trait divergence and speciation [19,20]. We note that this additional assumption reduces the number of viable genotypes to two, simplifying analytic treatments.

In what follows, we use g for n_{++} and h for n_{--} to make the notation concise. Similarly, the survival and reproductive rates for these types are denoted by σ_g, λ_g, σ_h, and λ_h. We restrict ourselves to symmetric cases only, in which two viable genotypes g and h share the same survival and reproductive rates, i.e., $\sigma_g = \sigma_h = \sigma$ and $\lambda_g = \lambda_h = \lambda$. Finally, we again measure the populations in units of the carrying capacity κ. With these assumptions Eq. (2) becomes

$$
\begin{aligned}
g'(\boldsymbol{x}) = \sigma g(\boldsymbol{x}) &+ \frac{\lambda \langle g(\boldsymbol{x}) \rangle_M^2}{\langle g(\boldsymbol{x}) + h(\boldsymbol{x}) \rangle_M} \\
&\times [1 - \langle g(\boldsymbol{x}) + h(\boldsymbol{x}) \rangle_C], \qquad (26)
\end{aligned}
$$

$$h'(x)=\sigma h(x)+\frac{\lambda\langle h(x)\rangle_M^2}{\langle g(x)+h(x)\rangle_M}\times[1-\langle g(x)+h(x)\rangle_C], \tag{27}$$

with the constraints $g\geqslant 0, h\geqslant 0$. Versions of this disruptive selection model have been used to study symmetry breaking and coarsening in spatially distributed populations [1] and stability analysis of polymorphic populations in reproduction-migration dynamics among semi-isolated demes [21]. We note that Eqs. (26) and (27) can be rewritten in terms of the total population density $n=g+h$, and what we call type difference $c\equiv g-h(-n\leqslant c\leqslant n)$, i.e.,

$$n'(x)=\sigma n(x)+\lambda\frac{\langle n(x)\rangle_M^2+\langle c(x)\rangle_M^2}{2\langle n(x)\rangle_M}\times[1-\langle n(x)\rangle_C], \tag{28}$$

$$c'(x)=\sigma c(x)+\lambda\langle c(x)\rangle_M[1-\langle n(x)\rangle_C]. \tag{29}$$

B. Homogeneous solutions

We first calculate the homogeneous solutions for the disruptive selection case, in the same way as for the previous flat fitness cases. For homogeneous populations the local averages over M and C can be ignored and Eqs. (26) and (27) are simplified to

$$g'=\sigma g+\lambda\frac{g^2}{g+h}[1-(g+h)], \tag{30}$$

$$h'=\sigma h+\lambda\frac{h^2}{g+h}[1-(g+h)]. \tag{31}$$

Stationary solutions are obtained by setting $g'=g$ and $h'=h$, resulting in the following four solutions:

$$g=h=0,$$

$$g=\frac{\sigma+\lambda-1}{\lambda}\equiv g_0,\quad h=0,$$

$$g=0,\quad h=\frac{\sigma+\lambda-1}{\lambda}\equiv h_0,$$

$$g=h=\frac{2\sigma+\lambda-2}{2\lambda}\equiv m_0.$$

In the (g,h) plane, these stationary solutions lie along the lines $h=0$, $g=0$, and $g=h$. These lines are invariant subspaces under the population dynamics, so that initial conditions starting on one of these lines remain on the same line. This allows us to consider the model behavior as a combination of the one-dimensional dynamics on each line and its stability against orthogonal perturbations to that line.

We first show that the dynamics restricted to the line $h=0$ or $g=0$ is the same as that in the flat fitness case. Setting $h=0$ or $g=0$, we find

$$g'=\sigma g+\lambda g(1-g) \tag{32}$$

or

$$h'=\sigma h+\lambda h(1-h), \tag{33}$$

which are the same as Eq. (4). This reflects the existence of only one genotype within the population along the lines $h=0$ or $g=0$, so that genetic inhomogeneity plays no role. Along these lines, the same stationary solutions (extinction and one-type dominance) and the same role of $\sigma+\lambda$ occur. These solutions are also stable to small perturbations away from the axes (introduction of the other type), because a minority type introduced into a population of another type, with which they cannot produce viable offspring, disappears exponentially. This can be derived by assuming $h\ll g\approx g_0$ (or $g\ll h\approx h_0$) in Eqs. (30) and (31), obtaining $h'\approx\sigma h(g'\approx\sigma g)$ with $\sigma<1$.

The mixed solution $g=h=m_0$ is best represented by Eqs. (28) and (29). For a homogeneous population we obtain

$$n'=\sigma n+\lambda\frac{n^2+c^2}{2n}(1-n), \tag{34}$$

$$c'=\sigma c+\lambda c(1-n). \tag{35}$$

The mixed solution is on the invariant line $c=0$. On this line Eq. (34) becomes

$$n'=\sigma n+\frac{\lambda n}{2}(1-n), \tag{36}$$

which differs from Eqs. (4), (32), and (33) only in that the net reproductive rate of this mixed solution is reduced by a factor of 2 due to disruptive selection. If we define $\beta\equiv\sigma+\lambda/2$ and $r\equiv\lambda n/(2\beta)$, Eq. (36) turns into the logistic equation

$$r'=\beta r(1-r). \tag{37}$$

Therefore, along this line, the solution $r=0$ $(g=h=0)$ is stable for $\beta<1$ and the solution $r=(\beta-1)/\beta$ $(g=h=m_0)$ is stable for $1<\beta<3$. We note that the mixed solution is unstable to perturbations in the orthogonal type-difference direction. By assuming $c^2\ll n^2$ and $n\approx 2m_0$, Eqs. (34) and (35) give $n'\approx n$ and $c'\approx(2-\sigma)c$. With $\sigma<1$, this implies exponential growth for small perturbations in type difference.

Combining these results, we find the following scenario for homogeneous populations in the disruptive selection

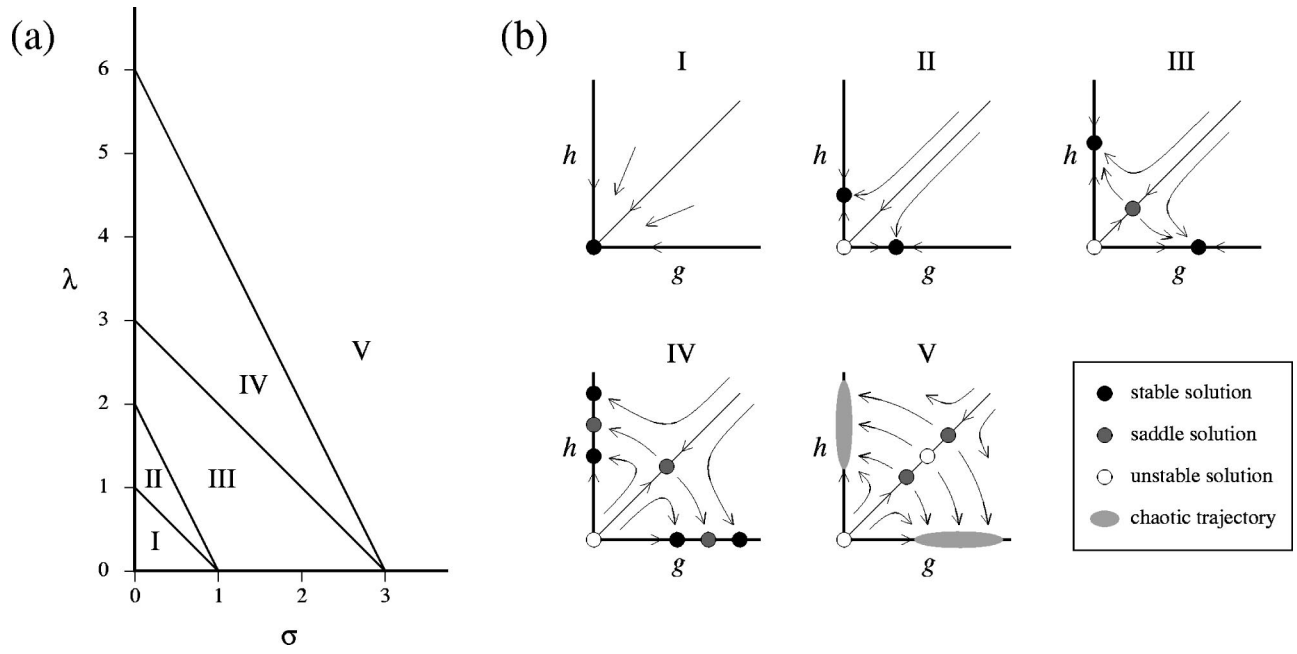

FIG. 4. (a) Five regimes in the (σ,λ) parameter space, drawn according to the existence and stability of four stationary solutions obtained from the homogeneous version of our model for disruptive selection cases. Note that only the regions with $\sigma<1$ are relevant to biological interpretations of the model. (b) Phase diagrams in the (g,h) plane for each regime (see text).

case. The (σ,λ) parameter space is divided into five regimes determining the existence and stability of the four stationary solutions (Fig. 4).

(I) $\sigma+\lambda<1$: only extinction is possible, as an attractor for any initial condition.

(II) $\sigma+\lambda>1$ and $\sigma+\lambda/2<1$: extinction is unstable along the lines $g=0$ and $h=0$, but not along the line $g=h$. The one-type dominant solutions are stable attractors.

(III) $\sigma+\lambda/2>1$ and $\sigma+\lambda<3$: the mixed solution $g=h=m_0$ is a saddle point. Extinction is unstable in all directions. The one-type dominant solutions are stable.

(IV) $\sigma+\lambda>3$ and $\sigma+\lambda/2<3$: the one-type dominant solutions undergo period-doubling bifurcations beginning at $\sigma+\lambda=3$, leading to chaos.

(V) $\sigma+\lambda/2>3$: the mixed solution undergoes period-doubling bifurcations beginning at $\sigma+\lambda/2=3$, leading to chaos. It continues to be unstable to type difference perturbations.

C. Stability analysis of the spatially extended version

We can conduct a linear stability analysis of pattern formation in both population density and type difference for the disruptive selection case, similar to the previous section. We will study the mixed solution only, because the dynamics of the one-type dominant solutions is the same as that of the flat fitness case, due to their robustness against type difference perturbation.

Adding a two-dimensional oscillatory perturbation to the mixed solution in the homogeneous population, we write

$$n^t(x,y)=2m_0+\zeta\nu^t s(x,y), \tag{38}$$

$$c^t(x,y)=0+\eta\nu^t s(x,y), \tag{39}$$

where ζ and η are small amplitudes and $s(x,y)$ is the same space-dependent perturbation [Eq. (7)] as used in the previous analysis. Substituting Eqs. (38) and (39) into Eqs. (28) and (29) and keeping only linear terms of ζ and η, the equations for these two variables decouple and we obtain

$$n^{t+1}(x,y)=2m_0+\zeta\nu^t[\sigma s(x,y)+(1-\sigma)\langle s(x,y)\rangle_M - (\sigma+\lambda/2-1)\langle s(x,y)\rangle_C], \tag{40}$$

$$c^{t+1}(x,y)=\eta\nu^t[\sigma s(x,y)+2(1-\sigma)\langle s(x,y)\rangle_M]. \tag{41}$$

Using the approximation in Eq. (9) for the local averages results in

$$\nu\zeta=[\sigma+(1-\sigma)A(fR_M) - (\sigma+\lambda/2-1)A(fR_C)]\zeta, \tag{42}$$

$$\nu\eta=[\sigma+2(1-\sigma)A(fR_M)]\eta, \tag{43}$$

with eigenvalues

$$\nu=\sigma+(1-\sigma)A(fR_M)-(\sigma+\lambda/2-1)A(fR_C) \tag{44}$$

for eigenvector $(\zeta,0)$, which we call the n direction, and

$$\nu=\sigma+2(1-\sigma)A(fR_M) \tag{45}$$

for eigenvector $(0,\eta)$, which we call the c direction.

Equation (44) is similar to Eq. (10), so we can apply the results of the previous stability analysis to the n direction, by replacing δ with $\hat{\delta}\equiv(\sigma+\lambda/2-1)/(1-\sigma)$. The regime for patterns to form in population density is thus exactly the same as shown in Fig. 2 if we view the ordinate as the $\hat{\delta}$ axis. The characteristic wavelength L is the same as before.

In terms of the c direction, however, the eigenvalue ν depends only on σ, R_M, and not on λ, R_C. Considering $|\nu|>1$ we obtain

$$A(fR_M)>\frac{1}{2}, \tag{46}$$

which numerically gives $fR_M<u_c\approx 2.215\,09$ (see Fig. 1). This means that any perturbation in the c direction whose wavelength is longer than the critical value

$$L_c\equiv 2\pi R_M/u_c\approx 2.836\,54R_M \tag{47}$$

destabilizes the homogeneous solution. This is the direction of type difference, $g=-h$, increasing g while decreasing h, or the reverse. Our result implies that all perturbations with shorter wavelengths than L_c are filtered out in an initial transient and then each local site tends to align with its neighbors at the scale L_c toward either genotype $[++]$ or $[--]$. Note that L_c depends only on the mating range and not on the competition range. This result is intuitive because it corresponds to the relevance of the mating range for genetic patterns and the competition range for population density variation. In the linear stability analysis, these two effects are found to be independent. However, an interplay between them arises once nonlinear effects become important. The details of this process will be discussed in the following section.

D. Genetic invasion

In this section, we consider the dynamics of genetic composition in the disruptive selection case and how it is affected by the spatial population structure created by competition. Disruptive selection causes a context-dependent dynamics, which gives rise to a subtle interplay between each spatially isolated group's own genetic evolution and genetic invasion from other groups. This usually results in coarsening of spatial patterns of genetic composition, but the specifics depend on the ratio of mating and competition ranges, γ. Our analysis shows that there are three critical values of γ, at which the behavior of the system changes from complete decoupling to incomplete decoupling to incomplete coarsening to complete coarsening.

1. Underlying dynamics

We first consider the dynamics of genetic composition with no significant population density variation. The update equation of the probability of one genotype can be obtained from Eqs. (28) and (29) by defining $p_g\equiv g/n=(n+c)/(2n)$ for sites where organisms exist $(n>0)$, which results in

$$p_g'(\boldsymbol{x})=p_g(\boldsymbol{x})+\frac{U(\boldsymbol{x})}{\sigma+U(\boldsymbol{x})}\times\left[\frac{[P_g^M(\boldsymbol{x})]^2}{[P_g^M(\boldsymbol{x})]^2+[1-P_g^M(\boldsymbol{x})]^2}-p_g(\boldsymbol{x})\right], \tag{48}$$

with

$$U(\boldsymbol{x})\equiv\frac{\lambda\langle n(\boldsymbol{x})\rangle_M}{n(\boldsymbol{x})}[1-\langle n(\boldsymbol{x})\rangle_C]\times\{[P_g^M(\boldsymbol{x})]^2+[1-P_g^M(\boldsymbol{x})]^2\}, \tag{49}$$

$$P_g^M(\boldsymbol{x})\equiv\frac{\langle g(\boldsymbol{x})\rangle_M}{\langle n(\boldsymbol{x})\rangle_M}=\frac{\langle n(\boldsymbol{x})+c(\boldsymbol{x})\rangle_M}{2\langle n(\boldsymbol{x})\rangle_M}. \tag{50}$$

$P_g^M(\boldsymbol{x})$ is the probability of genotype $[++]$ observed within M around $\boldsymbol{x}$. Equation (48) is quite similar in form to Eq. (19). For populations that do not exceed the carrying capacity, $U(\boldsymbol{x})/[\sigma+U(\boldsymbol{x})]$ is always positive and thus p_g always approaches the first term in the large square brackets, which is a typical update rule of allelic frequencies for populations with disruptive selection when there is no bias between the fitness of the two types [1]. The above equations are for genotype $[++]$ but they also apply to genotype $[--]$ due to the symmetry between the types.

Compared to the flat fitness case [Eq. (19)], the major change in Eq. (48) is that the first term in the large square brackets is no longer a conserved quantity even within the mean-field approximation. Its mean-field version is

$$p_g'=p_g+\frac{U}{\sigma+U}\left[\frac{p_g^2}{p_g^2+(1-p_g)^2}-p_g\right]=(1-\chi)p_g+\chi\frac{p_g^2}{p_g^2+(1-p_g)^2}, \tag{51}$$

where $\chi\equiv U/[\sigma+U]$. This form shows that p_g tends to go toward either 0 or 1, depending on whether its current value is larger or smaller than 1/2. $p_g=0$ and $p_g=1$ are the only possible stable solutions. Thus, any change in the average genetic composition within the mating neighborhood will not significantly affect the future genetic composition at the center of the neighborhood, unless the change is great enough to move the average composition across the value 1/2. Therefore, genetic invasion can occur only if there is a sufficiently large bias imposed on the local genetic composition from neighboring areas.

Figure 5 shows a numerical simulation of this process with parameter settings for which the homogeneous population density is stable. Disruptive selection causes each local

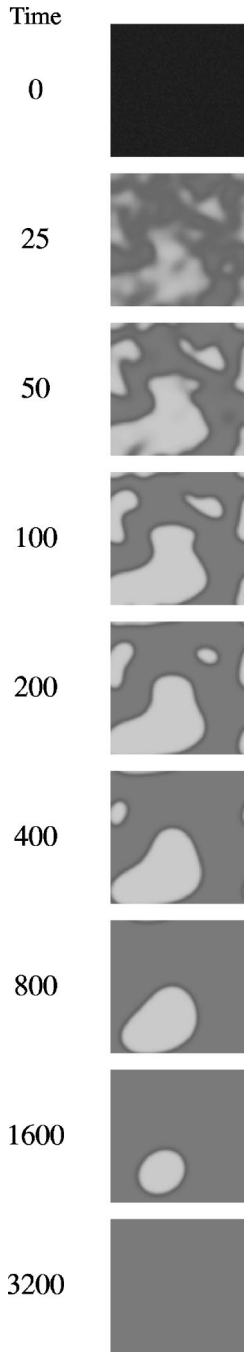

FIG. 5. Numerical simulation result of pattern formation in type difference in the disruptive selection case. The space consists of 128×128 sites with periodic boundary conditions. Each picture shows a configuration of the entire space. Dark gray represents the existence of $[++]$ organisms, while light gray represents the existence of $[--]$. The initial condition is a randomly generated population with $n=0.1\kappa$ (with $\pm0.02\kappa$ fluctuations) for each site. $\sigma=0.9$, $\lambda=0.7$, $R_M=5$, and $R_C=3$, so that $\hat{\delta}=2.5$ and $\gamma=1.666\,67$. This parameter setting falls into the regime where the homogeneous population density is stable (see Fig. 2) and thus no spatial separation occurs. The observed behavior is symmetry breaking and coarsening, which is found in systems with nonconserved order parameters, such as quenched Ising models.

region to assume either of the two fittest types, giving rise to symmetry breaking and formation of patterns of two different genotypes (light gray and dark gray shown in the figure). Once the patterns form, their subsequent evolution follows well-known coarsening behavior in systems where the order parameter is not conserved [22], e.g., quenched Ising models. The boundaries between the two types (called hybrid zones) move toward the direction determined by their local curvature, which acts as a bias on the local genetic composition. The characteristic wavelength of the patterns grows as $t^{1/2}$ [1]. In general, a population of finite size will eventually be dominated by one of the two types. Such coarsening dynamics is consistent with the eigenvalue ν in the c direction in Eq. (45), describing the instability of the mixed solution to type-difference perturbations. The value of ν monotonically increases as the wavelength of the perturbations increases for $L>L_c$, indicating that larger-scale perturbations become more apparent over longer times.

2. Genetic invasion between isolated groups

For populations spontaneously structured into spatially isolated groups, the spatial separation between the groups significantly affects the genetic invasion processes. When such isolation occurs, the ratio of the mating and competition ranges, γ, determines the possibility of genetic invasion.

We systematically consider this problem by dividing the local population within the mating neighborhood into two parts: a particular group at the center of the neighborhood, and the set of other groups that are spatially separated from the central group. Each part is represented by its total population. In a sense, this characterization corresponds to a mean-field approximation applied to the group-level description of the system. The total population and the probability of genotype $[++]$ within the focal group are denoted by n_{en} and P_g^{en}, and similarly, those outside the group by n_{ex} and P_g^{ex}. We consider how the genetic composition of the focal group P_g^{en} develops over time, assuming P_g^{ex}, n_{en}, and n_{ex} as environmental constants. In the context of coarsening in type difference, P_g^{ex} can be considered to represent the local curvature of boundaries between two types for the groups at or near the boundaries. This enables us to obtain implications for the coarsening behavior from this analysis.

We assume that each isolated group is genetically well mixed so that P_g^{en} is represented by the local probability p_g at the center of that group. From Eq. (48), p_g tends to approach $(P_g^M)^2/[(P_g^M)^2+(1-P_g^M)^2]$. P_g^M, the probability of genotype $[++]$ within the neighborhood, is written as

$$P_g^M=\frac{P_g^{\mathrm{ex}}n_{\mathrm{ex}}+P_g^{\mathrm{en}}n_{\mathrm{en}}}{n_{\mathrm{ex}}+n_{\mathrm{en}}}=P_g^{\mathrm{ex}}d+P_g^{\mathrm{en}}(1-d), \tag{52}$$

where $d\equiv n_{\mathrm{ex}}/[n_{\mathrm{ex}}+n_{\mathrm{en}}]$. d is the ratio between the subpopulation outside the focal group and the total population, within the neighborhood. Applying Eq. (52) to Eq. (48) and replacing p_g with P_g^{en}, we obtain a difference equation

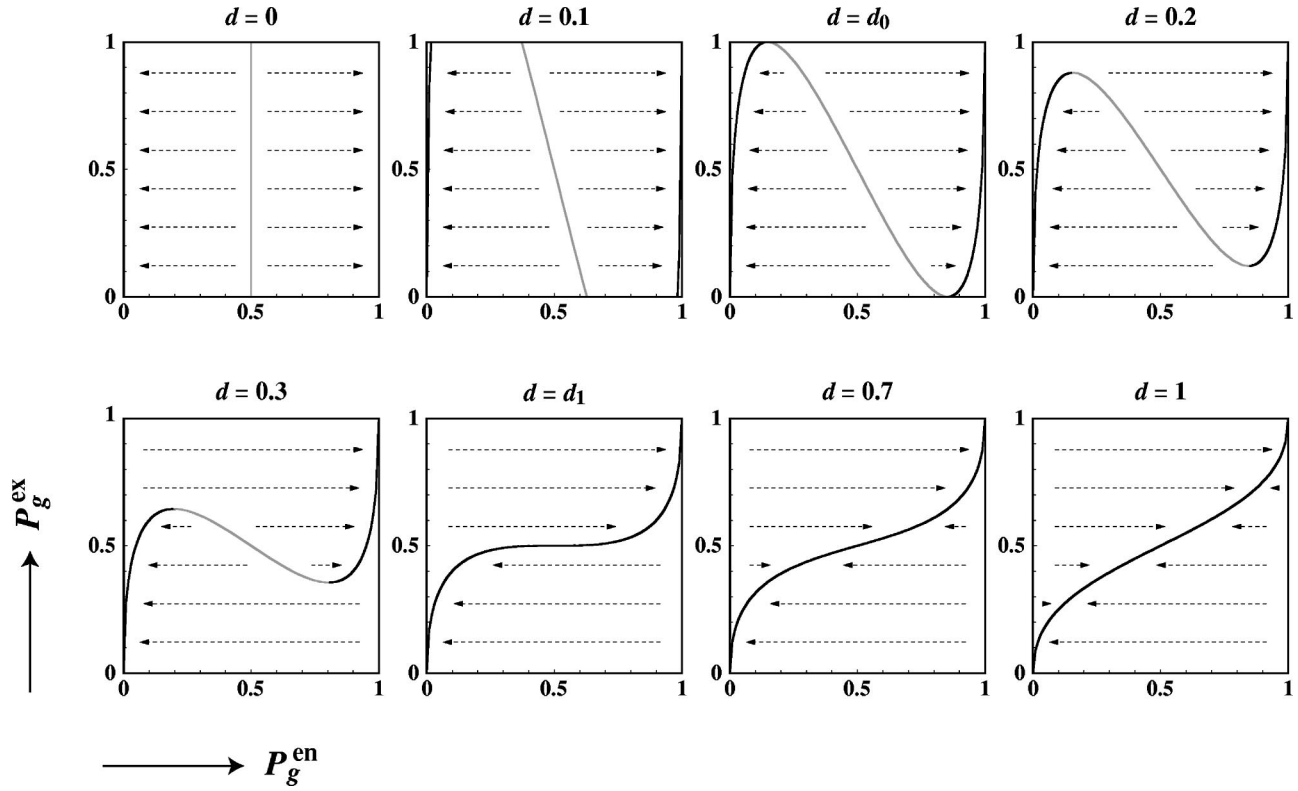

FIG. 6. Phase diagrams in the $(P_g^{\mathrm{en}},P_g^{\mathrm{ex}})$ plane for different values of d, obtained from Eqs. (54) and (55). The curves represent the solutions of $\Delta P_g^{\mathrm{en}}=0$. Black parts of the curves are stable and gray parts are unstable. For $d<d_0$, a group starting at or near $P_g^{\mathrm{en}}=0$ or 1 remains close to its original state almost regardless of P_g^{ex}. For $d_0<d<d_1$, genetic invasion is possible for sufficiently large (or small) P_g^{ex}. For $d>d_1$, genetic invasion always occurs since the final state of P_g^{en} is determined solely by P_g^{ex}, regardless of its original state. The actual values of d_0 and d_1 can be found analytically to be $d_0=3-2\sqrt{2}\approx 0.171\,573$ and $d_1=1/2$.

$$\Delta P_g^{\mathrm{en}}\equiv P_g^{\mathrm{en}\prime}-P_g^{\mathrm{en}}=\frac{U}{\sigma+U}\left[\frac{[P_g^{\mathrm{ex}}d+P_g^{\mathrm{en}}(1-d)]^2}{[P_g^{\mathrm{ex}}d+P_g^{\mathrm{en}}(1-d)]^2+[1-P_g^{\mathrm{ex}}d-P_g^{\mathrm{en}}(1-d)]^2}-P_g^{\mathrm{en}}\right]. \tag{53}$$

To study the possibility of genetic invasion, we consider when stable solutions of $\Delta P_g^{\mathrm{en}}=0$ exist for particular P_g^{ex} and d. We solve $\Delta P_g^{\mathrm{en}}=0$ with the restrictions $0\leqslant P_g^{\mathrm{en}}\leqslant 1$ and $0\leqslant P_g^{\mathrm{ex}}\leqslant 1$, which gives

$$P_g^{\mathrm{en}}=0,\quad \frac{1}{2},\quad 1 \tag{54}$$

for $d=0$, or otherwise

$$P_g^{\mathrm{ex}}=\begin{cases} P_g^{\mathrm{en}}+\dfrac{2P_g^{\mathrm{en}}(1-P_g^{\mathrm{en}})-\sqrt{P_g^{\mathrm{en}}(1-P_g^{\mathrm{en}})}}{d(2P_g^{\mathrm{en}}-1)} \\ \qquad (\text{for } P_g^{\mathrm{en}}\neq 1/2) \\ 1/2 \qquad (\text{for } P_g^{\mathrm{en}}=1/2), \end{cases} \tag{55}$$

which forms a continuous function that is differentiable for $0<P_g^{\mathrm{en}}<1$ including 1/2. Figure 6 shows phase diagrams in the $(P_g^{\mathrm{en}},P_g^{\mathrm{ex}})$ plane drawn from these solutions for different values of d. At $d=d_0$, a critical situation arises where the curve comes in contact with $P_g^{\mathrm{ex}}=0$ and $P_g^{\mathrm{ex}}=1$. At $d=d_1$, another critical situation is reached where the curve loses its unstable part. The actual values of d_0 and d_1 are analytically calculable, which results in $d_0=3-2\sqrt{2}\approx 0.171\,573$ and $d_1=1/2$.

From Fig. 6 we understand the following.

For $d=0$. The environment P_g^{ex} has absolutely no effect on the genetic composition of the focal group.

For $0<d<d_0$. A group with P_g^{en} close to 1/2 is sensitive to P_g^{ex}. However, a group starting at or near $P_g^{\mathrm{en}}=0$ or 1 cannot change to the opposite type due to the existence of intermediate stable solutions. Once an isolated group approaches dominance by either of the two fittest genotypes, genetic shift from one type to another is not possible regardless of P_g^{ex}.

For $d_0<d<d_1$. Genetic invasion is possible for P_g^{ex} larger (or smaller) than the local maximum (or minimum) of the curve. This indicates that the influx of a different genotype to the group must be greater than a threshold to cause genetic invasion. In the context of coarsening, boundaries whose lo-

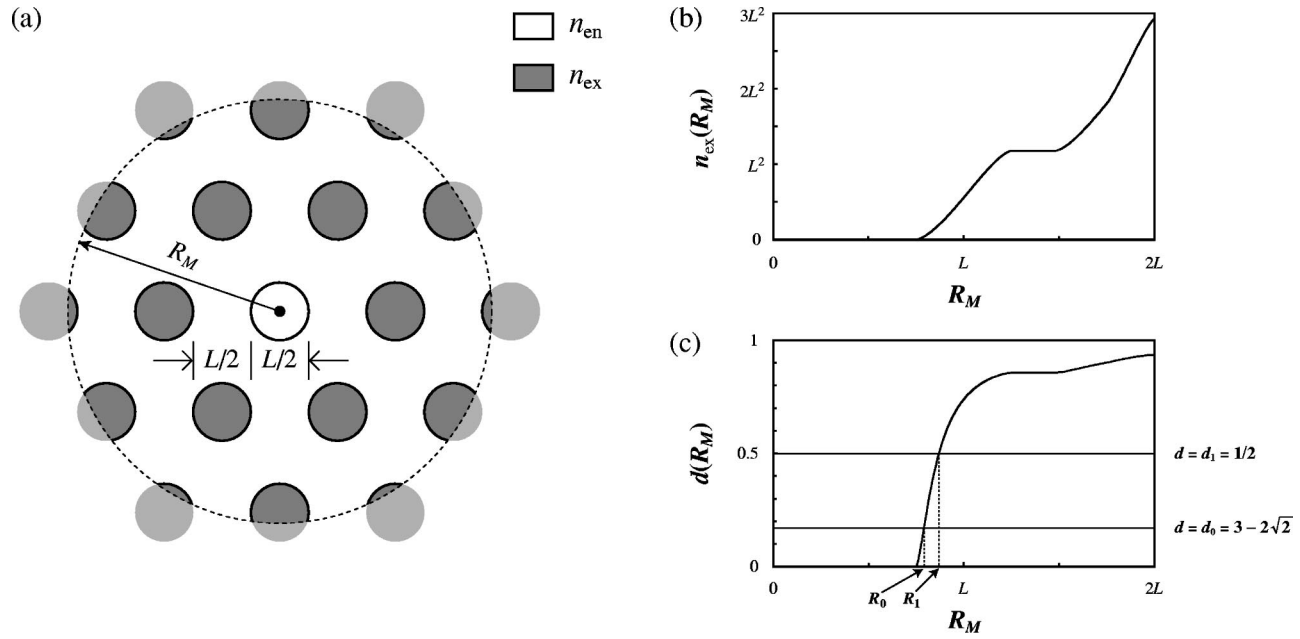

FIG. 7. (a) Illustration of the idealized group distribution assumed to compute d as a function of $\gamma = R_M / R_C$. The isolated groups are assumed to be arranged on a regular hexagonal lattice with basis vectors of length L and group diameter $L/2$. The population density is assumed to be flat within a group and thus the total population of a region is proportional to the populated area. n_{en} is the area of the central white circle $[n_{en} = \pi(L/4)^2]$, while n_{ex} is the total area of the gray regions. (b) A plot of n_{ex} as a function of R_M, drawn based on analytical calculation using the assumptions in (a). (c) A plot of d as a function of R_M, drawn from (b). Two critical points $d = d_0 = 3 - 2\sqrt{2}$ and $d = d_1 = 1/2$ are shown with the corresponding R_M values R_0 and R_1.

cal curvature is smaller than the threshold may be frozen, and in general will not become flat. The maximal curvature that can be kept from coarsening is determined by the values of P_g^{ex} at its extrema, which is a function of d.

For $d_1 < d$. P_g^{en} always converges toward a value determined solely by P_g^{ex}, regardless of its original state, thus genetic invasion always occurs. In the context of coarsening, any small curvature of boundaries can, in principle, give rise to change in genetic composition in the group at the boundaries, and coarsening continues until all the boundaries become flat or the entire population becomes dominated by one type.

3. The role of γ

The variable d is ultimately determined by the model parameter γ, the ratio of mating, and competition ranges. For large γ, the mating neighborhood extends over more groups, which increases d as well. Although the exact value of d is hard to obtain, we estimate it by using the assumptions that (1) groups are arranged on a regular hexagonal grid [Fig. 7(a)] as seen in the numerical simulations, and that (2) the population distribution within a group is uniform. With these assumptions, n_{en} is the circular area shown by white, and n_{ex} is the area shown by gray, in the figure. $n_{en} = \pi(L/4)^2$ for $R_M > L/4$. The algebraic solution gives $n_{ex}(R_M)$ plotted in Fig. 7(b), and $d(R_M)$ plotted in Fig. 7(c). The critical values of R_M such that $d = d_0 = 3 - 2\sqrt{2}$ and $d = d_1 = 1/2$, which we call R_0 and R_1, are also shown. Numerically we obtain

$$R_0 \approx 0.791\,234L \approx 0.968 R_C \equiv \gamma_0 R_C, \tag{56}$$

$$R_1 \approx 0.869\,629L \approx 1.06 R_C \equiv \gamma_1 R_C, \tag{57}$$

where the coefficients before R_C are the corresponding values of γ, which we call γ_0 and γ_1. Finally, we note that γ_c computed in the flat fitness case still applies to the disruptive selection case with no modification. The analysis discussed here applies to spot patterns. A similar analysis may be done for the stripe patterns that occur for small $\hat{\delta}$ (see Fig. 2).

Using the above results, the following scenario describes the role of γ in the genetic invasion processes in the disruptive selection case.

For $\gamma < \gamma_c$ *(complete decoupling).* Once spatial separation of groups takes place, organisms in one group are genetically decoupled from the rest of the population and each group's genetic composition evolves independently. This corresponds to the case where $d = 0$.

For $\gamma_c < \gamma < \gamma_0$ *(incomplete decoupling).* Some intergroup influence occurs; however, effective genetic decoupling between the groups occurs as soon as each of them becomes dominated by either of the two fittest types. A change from one dominant type to another is not possible.

For $\gamma_0 < \gamma < \gamma_1$ *(incomplete coarsening).* Coarsening occurs to some extent, but boundaries with curvatures below a threshold remain.

For $\gamma_1 < \gamma$ *(complete coarsening).* Genetic invasion always occurs and coarsening continues until all boundaries are flat or one type dominates the entire population.

These results are confirmed in Fig. 8, which presents numerical simulations in the disruptive selection case with several different values of γ, starting with the initial conditions

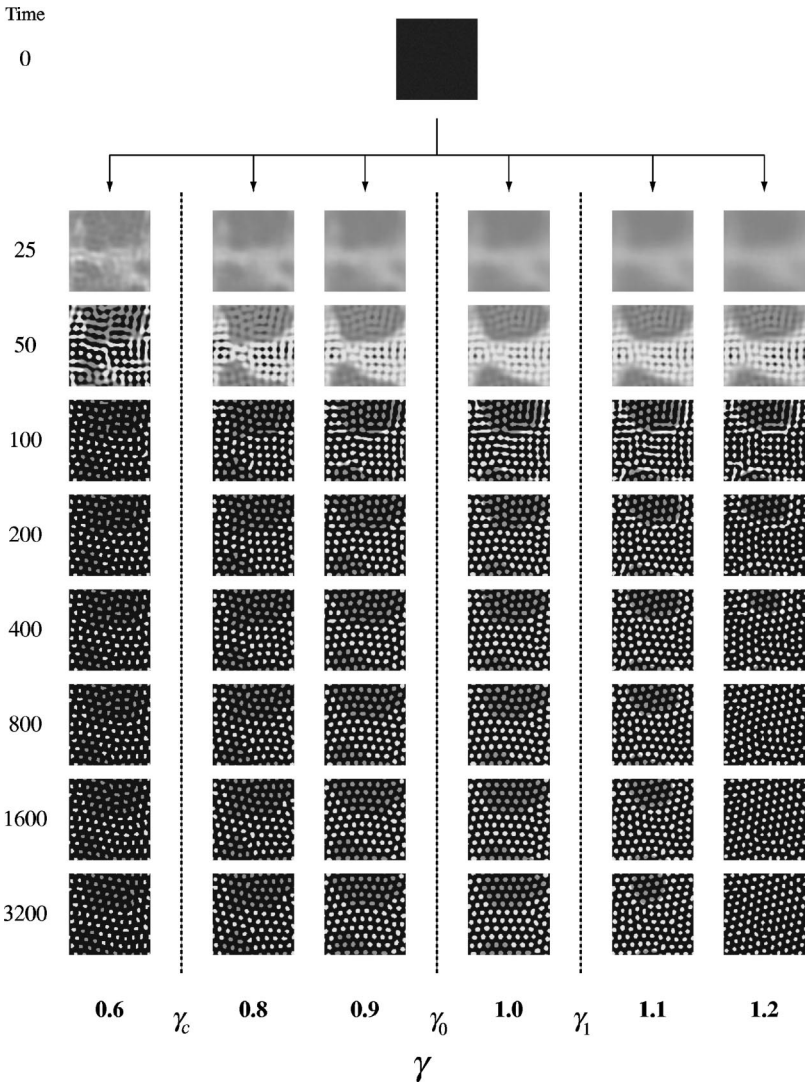

FIG. 8. Numerical simulations of pattern formation in both population density and type difference for several different values of γ in the disruptive selection case. The space consists of 128 $\times$128 sites with periodic boundary conditions. Each picture shows a configuration of the entire space. Dark gray represents the existence of $[++]$ organisms, light gray represents the existence of $[--]$, and black represents empty (or nearly empty) regions. $\sigma=0.9$ and $\lambda=3.0$ so that $\hat{\delta}=14$. R_C is fixed to 10, while R_M is varied to obtain different values of γ. The initial condition is a randomly generated population with $n=0.1\kappa$ (with $\pm 0.02\kappa$ fluctuations) for each site. The same initial condition is used for all cases to clarify the difference of behaviors for different γ. For $\gamma<\gamma_c\approx 0.612$, complete genetic decoupling occurs once groups are fully isolated from each other. For $\gamma_c<\gamma<\gamma_0\approx 0.968$, groups are effectively decoupled once they approach dominance by one of the two types (after about 200 updates). In contrast, for $\gamma>\gamma_1\approx 1.06$, coarsening continues after the isolation of groups, leading to eventual dominance of the whole population by one type. Between these regimes ($\gamma_0<\gamma<\gamma_1$) there is a distinct behavior where coarsening continues after the isolation of groups but stops when the local curvature of boundaries becomes below a threshold.

that are randomly created with small fluctuations in both population density and genetic composition. The effects of spatial separation on the coarsening behavior in type difference are seen to vary for different γ. For $\gamma<\gamma_0$, genetic decoupling actually occurs and thus coarsening stops after groups become fully isolated from each other (after about 200 updates), while for $\gamma>\gamma_1$, coarsening continues even after the isolation of groups and the whole population is eventually dominated by one type as predicted. Although this particular example does not clearly show how boundaries behave for $\gamma_0<\gamma<\gamma_1$, we can nonetheless observe a distinct behavior in other simulation runs where coarsening continues after the isolation of groups but eventually stops in a somewhat frustrated shape. Figure 9 shows another example, where isolated groups are already formed when disruptive selection events are induced. In this case, the difference between the cases $\gamma<\gamma_0$ and $\gamma>\gamma_1$ appears earlier due to the preexistence of the spatial separation. The final outcomes are similar to those in Fig. 8.

V. DISCUSSION

We have presented a theoretical analysis of evolutionary processes that involve organism distribution, genetic composition, and their interaction, for spatially distributed populations with local mating and competition. Analyses and numerical simulations reveal that the typical dynamics of population density variation is the formation of isolated groups (spots or stripes). This process depends on several parameters, including the reproduction rate and the survival rate of organisms and the ratio of mating and competition ranges. We have also found that the population density dynamics are sensitive to the shape of neighborhoods adopted. With well-defined competition neighborhoods groups may form, while with Gaussian neighborhoods they do not. This result implies that the spontaneously formed spatial population structure depends on the organismal behavior in marking their territories.

We have examined the dynamics of genetic composition under two different assumptions, the flat fitness case and the disruptive selection case. The former results in simple genetic diffusion, and the latter in symmetry breaking and coarsening. These genetic invasion processes may take place despite the spatial separation generated by competition. The observed dynamics fall into classes of system behaviors that have been studied in statistical physics, which illustrates their applicability to the quantitative understanding of bio-

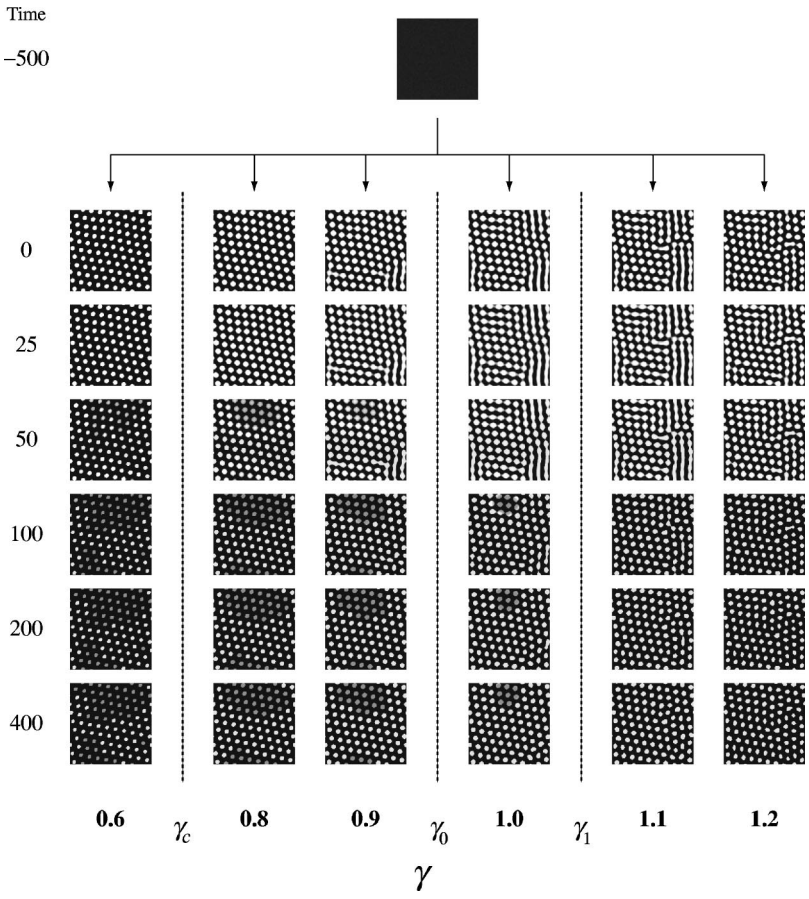

FIG. 9. Numerical simulations of pattern formation in type difference where disruptive selection is induced in a population which is already structured into isolated groups. As in Fig. 8, dark gray, light gray, and black indicate $[++]$, $[--]$, and empty regions, respectively. White represents a mixed population of all the possible genotypes. R_C is fixed to 10, while R_M is varied to obtain different values of γ. The conditions shown at time 0 are generated through 500 updates with $\sigma=0.9$ and $\lambda=1.5$ for all four genotypes (i.e., no disruptive selection) starting from the same initial population as used in Fig. 8. At time 0 the four possible genotypes all coexist in white groups. Then σ_{+-}, σ_{-+}, λ_{+-}, and λ_{-+} are all set to zero to cause disruptive selection, while λ_{++} and λ_{--} are increased to 3.0 to make $\hat{\delta}$ after the introduction of disruptive selection equal to δ before the introduction of disruptive selection. The behavioral difference between cases $\gamma<\gamma_0$ and $\gamma>\gamma_1$ appears earlier than the corresponding cases in Fig. 8, while the final outcomes are similar to those in Fig. 8.

logical population dynamics. There is an increasing interest in applying statistical models to evolutionary processes in the physics literature [23–31].

In a two-order-parameter system, the ratio of the characteristic length scales of these order parameters can be expected to play a crucial role in the dynamics. This corresponds to the ratio of the mating and competition ranges in the biological case we have discussed. When the ratio is larger than a critical value, significant intergroup migration takes place and genetic invasion ''jumps across'' the spatial gaps between the isolated groups. On the other hand, when the ratio is smaller than the critical value, genetic invasion does not occur and each group independently develops its own genetic composition. Such differences in behavior are relevant to the long-term evolution of the genetic composition of the population. The critical value of the ratio of the ranges, γ, is estimated to be about 0.6 for the flat fitness case. In the disruptive selection case, our analysis predicts that there are three distinct critical values of γ (one of them is the same as above), at which the behavior changes from complete decoupling to incomplete decoupling to incomplete coarsening to complete coarsening. In particular, in the incomplete coarsening regime where $\gamma\approx 1$ $(R_M\approx R_C)$, the coarsening of boundaries between different types may remain in a frustrated shape. These results are confirmed by numerical simulations. They may be verified by experimental observations in both qualitative and quantitative ways.

Finally, we point out that the formation of isolated groups and the possibility of lateral invasion of different types by migration over the groups seen in our results are of particular interest for discussion of the phase III of Wright's shifting balance theory [8,9]. Wright grappled with a problem of evolutionary improvement of fitness of sexually reproducing organisms crossing the valleys in fitness landscapes. He discussed the possibility of fitness improvement in the context of spatially distributed populations structured into small and nearly isolated demes that are weakly coupled by migration. In phase I of this process, random factors, such as mutations and fluctuations in selection, could cause a nearly isolated deme to develop its own genetic profile. In phase II, independent selection acting on each of the demes could bring some of them to a higher fitness peak. Then, in phase III, migration between demes could make it possible for the fitter genotype in certain demes to invade others. This theory (in particular its phase III process) has been the subject of a number of recent articles in theoretical population genetics [32–37]. The main concern that has been discussed is the calculation of a migration threshold beyond which invasion should occur. The models that have been considered involve biased migration rates and different numbers of loci, demes, and dimensions for the population distribution in physical space. These models, however, all share two common features: the assumption of the preexistence of isolated groups and the consideration of the possibility of invasion as resulting from fitness difference only.

In contrast, our model demonstrates an example of possible mechanisms of spontaneous formation of isolated groups due to competition, which enables us to consider the

ideas of Wright in a more self-consistent way. Moreover, it also shows the possibility of lateral invasion even with no significant fitness difference between two viable types ($\sigma_g = \sigma_h, \lambda_g = \lambda_h$). In this case the local curvature of boundaries between different types determines the direction of invasion, which corresponds to the difference in the local population size between the competing types. We present several more relevant local parameters that participate in the invasion processes elsewhere [21], among which the fitness difference is just one of the factors. These results imply that the simple but prevalent view of evolution as a hill climbing process acting on a fitness landscape must be corrected for more realistic contexts such as spatially extended populations. We believe that our model may provide a theoretical basis for further consideration of various complex properties of spatially extended evolutionary processes, which have not been captured by the conventional fitness-oriented perspectives on evolution.

There are a number of possible future extensions of the present model. We have previously considered more complex genetics with multiple loci and/or multiple alleles [7]. Another issue relevant to biological concerns is extending the fitness assignment to a more general form. A small asymmetry between fittest types or small viability of genetic intermediates may alter the model dynamics. Boundary shapes and behaviors could couple to fitness variation. Our discussions may also be used as an analog of some self-organization processes in physics that involve two or more order parameters, such as clustering and magnetization of aggregates of mobile spins on a two-dimensional surface, or pattern formation of chemical substrates in a reaction-diffusion system that involves multiple distinct reaction processes.

ACKNOWLEDGMENTS

M.A.M.A. acknowledges financial support from the Brazilian agencies FAPESP and CNPq. The work at the Center for Theoretical Physics was supported partially by the U.S. Department of Energy (DOE) under Contract No. DE-FC02-94ER40818.

[1] H. Sayama, L. Kaufman, and Y. Bar-Yam, Phys. Rev. E **62**, 7065 (2000).
[2] S. A. Levin and L. A. Segel, SIAM Rev. **27**, 45 (1985).
[3] R. Durrett and S. A. Levin, Philos. Trans. R. Soc. London, Ser. B **343**, 329 (1994).
[4] *Spatial Ecology: The Role of Space in Population Dynamics and Interspecific Interactions*, edited by D. Tilman and P. Kareiva (Princeton University Press, Princeton, NJ, 1997).
[5] A. S. Gandhi, S. Levin, and S. Orszag, J. Theor. Biol. **192**, 363 (1998).
[6] A. S. Gandhi, S. Levin, and S. Orszag, J. Theor. Biol. **200**, 121 (1999).
[7] H. Sayama, L. Kaufman, and Y. Bar-Yam (unpublished).
[8] S. Wright, Genetics **16**, 97 (1931).
[9] S. Wright, Am. Nat. **131**, 115 (1988).
[10] R. May, Nature (London) **261**, 459 (1976).
[11] M. J. Feigenbaum, J. Stat. Phys. **19**, 25 (1978).
[12] A. Turing, Philos. Trans. R. Soc. London, Ser. B **237**, 37 (1952).
[13] J. D. Murray, J. Theor. Biol. **88**, 161 (1981).
[14] D. Young, Math. Biosci. **72**, 51 (1984).
[15] Y. Bar-Yam, *Dynamics of Complex Systems* (Perseus Books, Reading, MA, 1997), Chap. 7.
[16] J. Dethier, F. Baras, and M. M. Mansour, Europhys. Lett. **42**, 19 (1998).
[17] A. Lipowski, Phys. Rev. E **60**, 5179 (1999).
[18] J. M. Thoday, Philos. Trans. R. Soc. London, Ser. B **182**, 109 (1972).
[19] A. S. Kondrashov and F. A. Kondrashov, Nature (London) **400**, 351 (1999).
[20] U. Dieckmann and M. Doebeli, Nature (London) **400**, 354 (1999).
[21] M. A. M. de Aguiar, H. Sayama, E. Rauch, Y. Bar-Yam, and M. Baranger, Phys. Rev. E **65**, 031909 (2002).
[22] A. J. Bray, Adv. Phys. **43**, 357 (1994).
[23] I. Aranson, L. Tsimring, and V. Vinokur, Phys. Rev. Lett. **79**, 3298 (1997).
[24] F. Bagnoli and M. Bezzi, Phys. Rev. Lett. **79**, 3302 (1997).
[25] A. Aafif and J. Lin, Phys. Rev. E **57**, 2471 (1998).
[26] P. Sibani and A. Pedersen, Europhys. Lett. **48**, 346 (1999).
[27] A. Lipowski, Phys. Rev. E **61**, 3009 (2000).
[28] V. M. de Oliveira and J. F. Fontanari, Phys. Rev. Lett. **85**, 4984 (2000).
[29] A. Pekalski and K. Sznajd-Weron, Phys. Rev. E **63**, 031903 (2001).
[30] M. A. Harrison, Y. C. Lai, and R. D. Holt, Phys. Rev. E **63**, 051905 (2001).
[31] A. Colato and S. S. Mizrahi, Phys. Rev. E **64**, 011901 (2001).
[32] J. F. Crow, W. R. Engels, and C. Denniston, Evolution (Lawrence, Kans.) **44**, 233 (1990).
[33] N. H. Barton, Evolution (Lawrence, Kans.) **46**, 551 (1992).
[34] S. Gavrilets, Evolution (Lawrence, Kans.) **50**, 1034 (1996).
[35] P. C. Phillips, Evolution (Lawrence, Kans.) **50**, 1334 (1996).
[36] K. A. Lythgoe, Genet. Res. **69**, 49 (1997).
[37] J. A. Coyne, N. H. Barton, and M. Turelli, Evolution (Lawrence, Kans.) **51**, 643 (1997).